A&A 398, 203–211 (2003)
DOI: 10.1051/0004-6361:20021577
© ESO 2003

Astronomy & Astrophysics

High-resolution X-ray spectroscopy of τ Scorpii (B0.2V) with *XMM-Newton*⋆

R. Mewe[1], A. J. J. Raassen[1,2], J. P. Cassinelli[3], K. A. van der Hucht[1], N. A. Miller[3], and M. Güdel[4]

[1] SRON National Institute for Space Research, Sorbonnelaan 2, 3584 CA Utrecht, The Netherlands
[2] Astronomical Institute "Anton Pannekoek", Kruislaan 403, 1098 SJ Amsterdam, The Netherlands
[3] Dept. of Astronomy, University of Wisconsin at Madison, 6251 Sterling Hall, North Charter Str., Madison, WI 53706, USA
[4] Paul Scherrer Institut, Würenlingen & Villigen, 5232 Villigen PSI, Switzerland

Received 24 July 2002 / Accepted 30 October 2002

Abstract. We report the analysis of the first high-resolution X-ray spectrum of the B0.2V star τ Scorpii obtained with the Reflection Grating Spectrometers (RGS) and the EPIC-MOS CCD spectrometers on board *XMM-Newton*. The spectrum exhibits bright emission lines of the H- and He-like ions of C, N, O, Ne, Mg, and Si, as well as Fe XVII & Fe XVIII lines. Line fluxes have been determined. Simultaneous fits to the RGS and EPIC spectra were used to obtain four plasma temperatures, emission measures, and the overall elemental abundances. This multi-temperature fitting yielded temperatures of 1.6, 5.2, 8.2, and $\gtrsim$20 MK. These temperatures are confirmed by DEM modelling. The nitrogen lines are relatively strong: the N/O abundance ratio is about 3× solar. No indication of a solar-type "FIP effect" was found for the other elements. According to the derived models the X-ray luminosity in the energy range 0.3–10 keV is $L_x = 3.2 \times 10^{31}$ erg s^{-1} at a distance of 132 pc. The sensitivity of the He-like forbidden and intercombination lines to a strong ultraviolet radiation field is used to derive upper limits to the radial distances at which lines of Mg XI, Ne IX, O VII, and N VI originate. The results suggest that the soft X-rays ($\lesssim$8 MK) originate from shocks low in the wind that are produced by the common mechanism of radiation line-driven instabilities. This is consistent with the observed emission line profiles that are much narrower ($\lesssim$500 km s^{-1}) than the broad lines (up to 1500 km s^{-1}) observed high up in the wind of ζ Puppis. The hot (~20–40 MK) component may be explained by a model involving dense clumps embedded in a wind which sweeps past them at high relative velocity (~1400–1700 km s^{-1}). Such an interaction would produce the strong shocks required.

Key words. stars: individual: τ Scorpii – stars: coronae – stars: early-type – stars: abundances – X-rays: stars

1. Introduction

Ever since space astronomy observations have been made, the MK standard main-sequence star τ Sco (HD 149438, B0.2V, Walborn & Fitzpatrick 1990) has been a target of importance and surprises. It is the latest of a sequence of OB stars that show O VI superionization (Lamers & Rogerson 1978) caused by X-ray ionization and the Auger ionization effect (Cassinelli & Olson 1979). Because of this, it has played a crucial role in the original prediction that OB stars would be X-ray sources.

τ Sco turned out to be a star with a harder X-ray spectrum than usual for B0V stars, as observed by *ROSAT* (Cassinelli et al. 1994; Cohen et al. 1997a) and *ASCA* (Cohen et al. 1997b). Its X-ray emission is very strong for its spectral subtype. The star τ Sco is at a distance of 132 pc as measured by Hipparcos (Perryman et al. 1997), and has a $T_{\rm eff}$ of 32 000 K. Using the *ASCA* (0.8–1.2 keV) measurements of Cohen et al. (1997a) with a corrected distance (see Howk et al. 2000) indicates that τ Sco has an X-ray luminosity of L_x = 1.8 × 10^{31} erg s^{-1} and a large $\log L_x/L_{\rm bol}$ of –6.53. In the *ROSAT* energy band (0.1–2.4 KeV), the intrinsic X-ray luminosity is 7.3 × 10^{31} erg s^{-1} and an even larger value of $\log L_x/L_{\rm bol} \simeq -5.93$ is measured. Explanations for these observational anomalies are still being explored. On the basis of τ Sco's O VI lines, which show evidence for some infalling material, and its hard X-ray flux, it has been suggested that clumps form in the wind, stagnate and fall inward. Because of the high shock velocity that this model predicts, the temperatures in the wind can be unusually high (Howk et al. 2000).

The *XMM-Newton* RGS and EPIC observations of τ Sco presented here allow an improvement in the determination of its X-ray luminosity and temperature structure, and a first independent abundance determination of the elements C, N, O, Ne and Fe. The observed element ionization stages C VI, N VI,

Send offprint requests to: R. Mewe, e-mail: r.mewe@sron.nl

⋆ Based on observations obtained with *XMM-Newton*, an ESA science mission with instruments and contributions directly funded by ESA Member States and the USA (NASA).

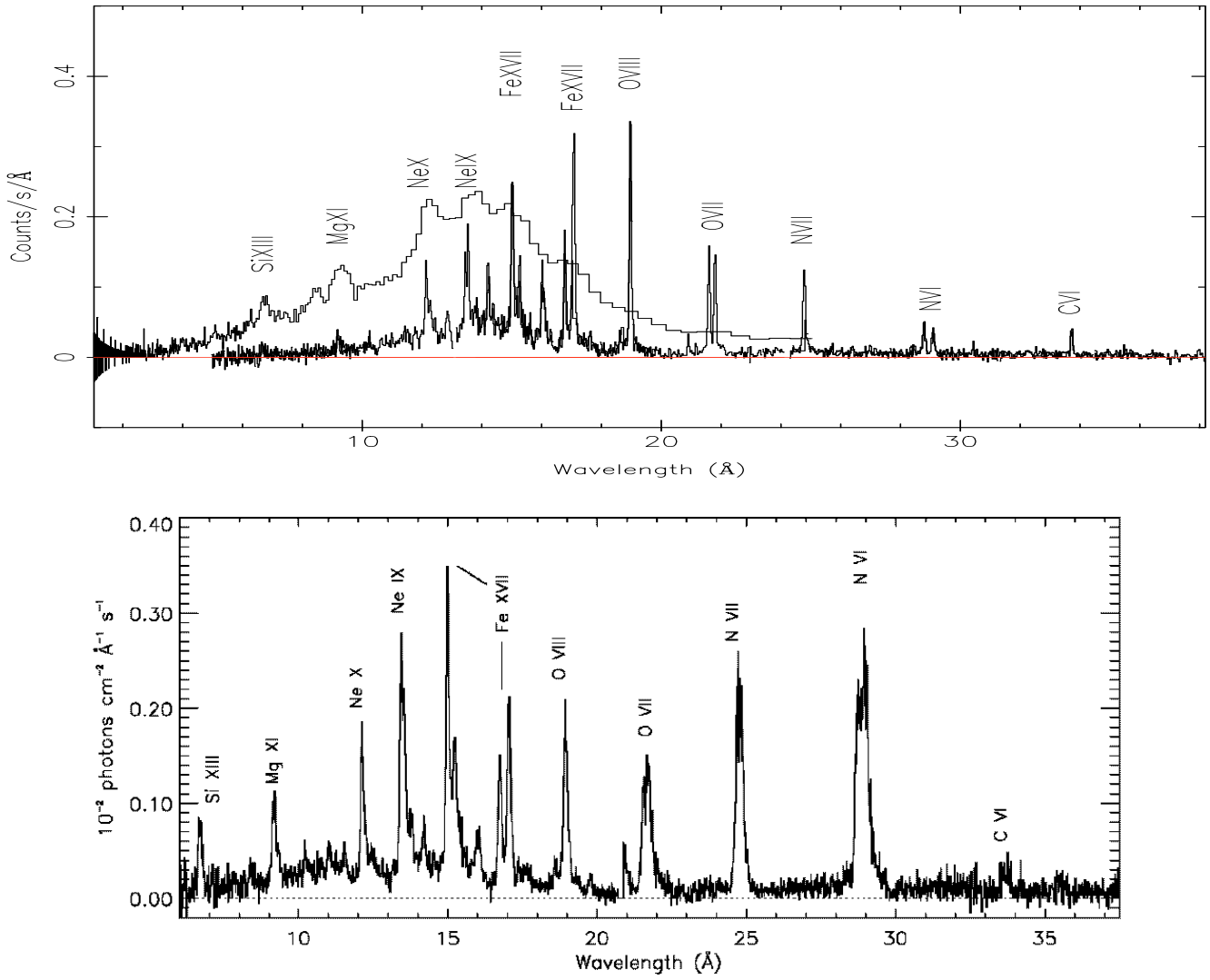

Fig. 1. Top panel: First-order background-subtracted spectrum of τ Sco observed by RGS (5–37 Å; rebinned by a factor 3) and the spectrum of the EPIC-MOS (1–25 Å). The spectra are not corrected for the effective areas of the instruments to show the different efficiencies. Several prominent lines are labelled with the emitting ions. Note the relatively high nitrogen flux. **Bottom panel**: ζ Pup *XMM*-RGS spectrum (from Kahn et al. 2001) for comparison to show the much broader lines and the even higher nitrogen line fluxes.

N VII, O VII, O VIII, Ne IX, Ne X, Fe XVII and Fe XVIII place strong constraints on the structure of the X-ray forming regions of the star, and provide crucial tests for understanding the nature of the source of X-ray emission from this important early-type star.

2. Observations

The spectra of τ Sco were obtained during 22.5ks (on August 20, 2001) with the *XMM-Newton* Reflection Grating Spectrometer (RGS) (Jansen et al. 2001) and with the EPIC-MOS (Turner et al. 2001) and -PN detectors (Strüder et al. 2001). The RGS covers the wavelength range 5 to 37 Å with a resolution of about 0.07 Å, and a maximum effective area of about 140 cm^2 around 15 Å.

The first RGS spectral order has been selected by means of the energy resolution of the CCD detectors (see den Herder et al. 2001). The data were processed with the *XMM-Newton* Science Analysis Software (SAS) system. The background spectrum was obtained by taking events from a region spatially offset from the source.

3. Data analysis

3.1. Determination of line fluxes

In Fig. 1, both the RGS spectra and the EPIC-MOS spectrum are plotted together. Table 1 shows the prominent lines. Note the relatively large nitrogen line flux relative to the oxygen (and carbon) lines reflecting an unusually large N/O abundance ratio.

The stronger spectral lines have been measured individually by folding delta functions through the instrumental response functions in order to derive the integrated line fluxes. A constant "background" level was adjusted in order to account for the real continuum and for the pseudo-continuum created by the overlap of several weak, neglected lines. In Table 1, we have

Table 1. Wavelengths and fluxes for RGS1+RGS2 and EPIC-MOS, together with line identifications.

RGS1		RGS2		EPIC-MOS		Line identifications[a]		
λ(Å)	flux[b]	λ(Å)	flux[b]	λ(Å)	flux[b]	λ(Å)	flux[c]	Ion
—	—	—	—	1.86(8)	$\lesssim$0.02[d]	1.86	0.006	Fe XXV w,y,z
—	—	—	—			1.86	0.005	Fe XXIV k,j,q
—	—	—	—	4.0(2)	0.05(4)	3.97	0.033[e]	Ar XVII w,y,z
—	—	—	—			3.97	0.018[e]	Ar XVI Lis
—	—	—	—	5.1(2)	0.14(4)	5.05	0.076	S XV w,y,z
—	—	—	—			5.06	0.027	S XIV Lis
—	—	—	—			5.220	0.024	Si XIV Lyβ
—	—	—	—	6.3(2)	0.17(4)	6.183	0.194	Si XIV Lyα
—	—	—	—	6.7(2)	0.56(7)	6.648	0.327	Si XIII w
—	—	—	—			6.65	0.093	Si XII Lis
—	—	—	—			6.688	0.082	Si XIII y
—	—	—	—			6.704	0.063	Si XII Lis
—	—	—	—			6.740	0.179	Si XIII z
—	—	—	—	—	—	7.105	0.051	Mg XII Lyβ
—	—	—	—	8.5(2)	0.23(7)	8.421	0.539	Mg XII Lyα
—	—	—	—			8.42	0.047	Mg XI Hes
—	—	9.189(14)	0.65(27)	9.3(3)	0.62(11)	9.170	0.552	Mg XI w
—	—	—	—			9.18	0.050	Mg XI Lis
—	—	—	—			9.232	0.186	Mg XI y
—	—	—	—			9.315	0.269	Mg XI z
10.241(14)	0.52(18)	10.255(36)	0.24(19)	—	—	10.239	0.18	Ne X Lyβ
gap	—	12.142(9)	2.0(2)	12.4(4)	3.1(2)	12.134	2.5	Ne X Lyα
gap	—	12.273(9)	1.0(2)			12.264	1.3	Fe XVII
gap	—					12.286		Fe XXI,XX
gap	—	13.453(9)	1.5(3)	13.6(4)	4.6(3)	13.448	1.1	Ne IX w
gap	—	13.546(9)	2.1(3)			13.521	1.5	Fe XIX
gap						13.553	0.49	Ne IX y
gap	—	13.658(36)	0.4(2)			13.798	0.4	Fe XIX
gap	—	13.822(21)	0.5(2)			13.826	0.5	Fe XVII
14.215(5)	1.6(2)	14.231(12)	0.8(2)	—	—	14.212	2.0	Fe XVIII
						14.260	0.4	Fe XVIII
—	—	14.391(16)	0.5(2)	—	—	14.374	0.5	Fe XVIII
15.028(5)	4.1(3)	15.022(3)	4.3(3)	14.9(4)	5.8(4)	15.013	5.7	Fe XVII[f]
15.203(18)	0.8(4)	15.205(21)	0.9(6)			15.176	0.18	O VIII Lyγ
						15.210	0.19	Fe XIX
15.269(14)	1.0(3)	15.268(10)	1.0(5)			15.265	1.55	Fe XVII
—	—	15.612(14)	0.6(2)	—	—	15.623	0.4	Fe XVIII
16.027(9)	1.7(2)	16.043 (9)	2.2(3)	—	—	16.006	0.7	O VIII Lyβ
						16.002	0.4	Fe XVIII
						16.078	1.2	Fe XVIII
16.777(5)	2.1(2)	16.777(6)	2.5(2)	16.8(4)	1.1(5)	16.780	2.9	Fe XVII
17.068(9)[g]	5.1(4)	17.059(14)	3.0(11)	—	—	17.055	3.3	Fe XVII
		17.092(14)	3.4(9)	—	—	17.100	2.6	Fe XVII
18.636(10)	0.3(1)	18.637(23)	0.4(1)	—	—	18.627	0.3	O VII
18.972(4)	5.4(3)	18.987(14)	5.5(3)	—	—	18.969	6.8	O VIII Lyα
20.914(16)	0.44(12)	gap	—	—	—	20.910	0.3	N VII Lyβ
21.169(19)	0.22(10)	gap	—	—	—	21.143	?	Ca XVII?
21.601(10)	2.6(6)	gap	—	—	—	21.602	3.0	O VII w
21.800(11)	2.7(6)	gap	—	—	—	21.804	2.7	O VII y
22.098(11)	$\lesssim$0.22[d]	gap	—	—	—	22.101	—	O VII z
24.791(15)	1.8(7)	24.776(13)	2.7(3)	—	—	24.781	3.1	N VII Lyα
28.468(17)	0.1(1)	28.46(11)	0.2(1)	—	—	28.466	0.20	C VI Lyβ
28.780(10)	1.2(2)	28.794(9)	1.1(2)	—	—	28.787	1.5	N VI w
29.096(14)	0.9(2)	29.087(9)	1.0(2)	—	—	29.084	1.4	N VI y
29.524(6)	$\lesssim$0.23[d]	29.520(8)	$\lesssim$0.23[d]	—	—	29.534	—	N VI z
33.716(14)	1.2(3)	33.723(9)	1.2(3)	—	—	33.736	2.0	C VI Lyα

[a] Identifications from Kelly (1987) and MEKAL (Mewe et al. 1985); w,y,z: He-like resonance, intercombination, and forbidden line, respectively; Lis and k,j,q: Li-like satellites; Hes: He-like satellites; Lyα,β,γ: H-like resonance lines.
[b] Observed flux in 10^{-4} photons cm^{-2} s^{-1}; values in parentheses are statistical 1σ uncertainties in the last digits.
[c] Model flux in 10^{-4} photons cm^{-2} s^{-1}, obtained from 4-T fitting of RGS+MOS spectra (see Sect. 3.3.1. and Table 2).
[d] 2σ upper limit derived from the background noise (cf. Fig. 3).
[e] 5-T fit with enhanced Ar abundance.
[f] Blended with Fe XVI satellite lines.
[g] Bad pixel.

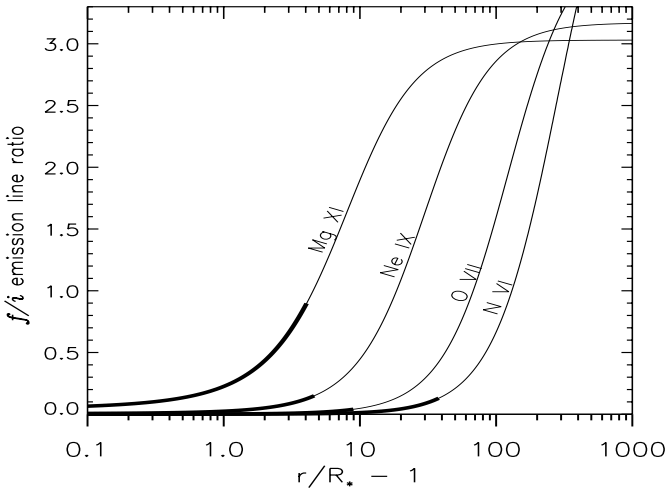

Fig. 2. Thin lines show expected f/i line ratio as a function of radius for the labeled He-like ions. The thickened portion of each line gives the radial range of the X-ray emission implied by the measured f/i line ratios.

collected the measured wavelengths and fluxes of the emission lines in the RGS instruments together with those in the EPIC-MOS.

3.2. Analysis of He-like spectral lines

Gabriel & Jordan (1969) were the first to demonstrate that forbidden (f), intercombination (i) and resonance (r) lines of the He-like "complexes" provide useful diagnostics for X-ray emitting plasmas. The most recent studies including the effects of dielectronic satellite lines and a radiation field have been done by Porquet et al. (2001). The ratio f/i is dependent on electron density because of the depopulation of the upper level of the f line at increasing density and can be used to derive electron densities in circumstances where radiation fields are relatively weak, such as in cool stars. However, in OB stars where the radiation fields are much stronger the depopulation of the upper level of the forbidden line then occurs by radiative absorption (e.g., Blumenthal et al. 1972; Porquet et al. 2001) and the f/i ratio no longer indicates the density, but instead provides information on the mean intensity of the radiation field, hence the radial distance of the X-ray source from the star.

The fact that the radiation field is the dominant effect for τ Sco is confirmed by detailed calculations. We use the stellar parameters for τ Sco taken from Howk et al. (2000): $T_{\rm eff}$ = 31 400 K, $R_* = 6.5\ R_\odot$, $\dot{M} = 3.1 \times 10^{-8}\ M_\odot\ {\rm yr}^{-1}$, v_∞ = 2400 km s^{-1}, and wind parameter $\beta = 0.8$ (see Eq. (2)). For the four He-like ions which allow reliable measurements of their f/i line ratio (N VI, O VII, Ne IX, Mg XI), these parameters indicate that τ Sco's radiation field will suppress the forbidden lines by radiative de-excitation of the upper level of f to much greater radii than would be possible with collisions (see, e.g., Waldron & Cassinelli 2001; Kahn et al. 2001; Cassinelli et al. 2001). Thus the expected f/i ratios as functions of radii for these four ions in Fig. 2 are entirely determined by τ Sco's radiation field. We use for the photospheric flux of τ Sco the continuum fluxes from a Kurucz model (Kurucz 1993). The forbidden line is nearly suppressed for all four ions. The 1σ upper limits derived from the RGS spectra for N VI, O VII, Ne IX, and Mg XI are: $f/i \lesssim 0.13$, $\lesssim 0.04$, $\lesssim 0.15$, $\lesssim 0.9$, respectively. Upper limits on the f/i ratios result in upper limits to the radial ranges r of the X-ray emission, which are: $\lesssim 40\ R_*$, $\lesssim 10\ R_*$,$\lesssim 5.5\ R_*$, and $\lesssim 5\ R_*$, respectively. Taken in the aggregate, these measurements strongly suggest that the bulk of the X-ray emission is emitted from regions relatively near the wind base.

3.3. Global fitting and emission measure modelling

We have determined the thermal structure and the elemental composition of τ Sco's X-ray emitting regions by means of multi-temperature fitting and by DEM-modelling of the spectrum as a whole.

3.3.1. Multi-temperature fitting

We fitted multi-T models of the spectra (RGS+MOS) using SPEX (Kaastra et al. 1996a). The spectral code in SPEX is based on the optically thin Collision Ionization Equilibrium (CIE) plasma model MEKAL (Mewe-Kaastra-Liedahl) as developed by Mewe et al. (1985, 1995). A broad range in plasma temperatures was obtained. For doing the fitting, the spectra were rebinned and cut off below about 9 Å for the RGS and above about 15.5 Å for the EPIC-MOS (see Fig. 3). In the multi-temperature calculations we have used four components; the temperatures and the corresponding EM values are given in Table 2 (2nd column), along with the abundances. The abundances are relative to solar photospheric values from Anders & Grevesse (1989) except for Fe, for which (instead of 7.67) we used log $A_{\rm Fe}$ = 7.50 (from Grevesse & Sauval 1998, 1999). In Table 2 we give in units of 10^{31} erg s^{-1} the X-ray luminosity $L_{\rm x}$ derived from the 4-T model in the *XMM* band (value 3.24) and for comparison also in the *ASCA* band (1.86) and the *ROSAT* band (4.0). The *ASCA* value is nearly the same as the measured *ASCA* value (1.73, cf. Sect. 1) but the *ROSAT* value is somewhat lower than that measured by *ROSAT* (7.3). However, this can be explained by the fact that a significant part of the soft X-ray flux measured by *ROSAT* between 0.1–0.3 keV cannot be detected by the RGS.

The hot component. We tested the robustness of the high-temperature component of our global 4-component model fit. If we refit the spectra with only three temperatures we obtain within the errors the same values for the temperatures, emission measures, and abundances, but the goodness of the 3-T fit ($\chi^2_{\rm red}$=1707/1022) is a little worse than the 4-T fit at the 2.5σ level ($\Delta\chi^2 = 112 \simeq 2.5 \times \sqrt{2 \times 1022}$). The two middle temperatures T_2 and T_3 are now combined into one temperature of 7 MK with the same total emission measure, but what is important is that the hot (20 MK) component is still retained. The latter is required to fit both the EPIC continuum plus some of the hotter lines (e.g., Si XIV, Mg XII) above a photon energy of $E \approx 1.5$ keV.

A sensitive test for the presence of a very hot component would in principle be the detection of an Fe-K feature at 6.7 keV. However, Fig. 3 shows that the hottest component of the 4-T best-fit model predicts an iron feature at 6.7 keV

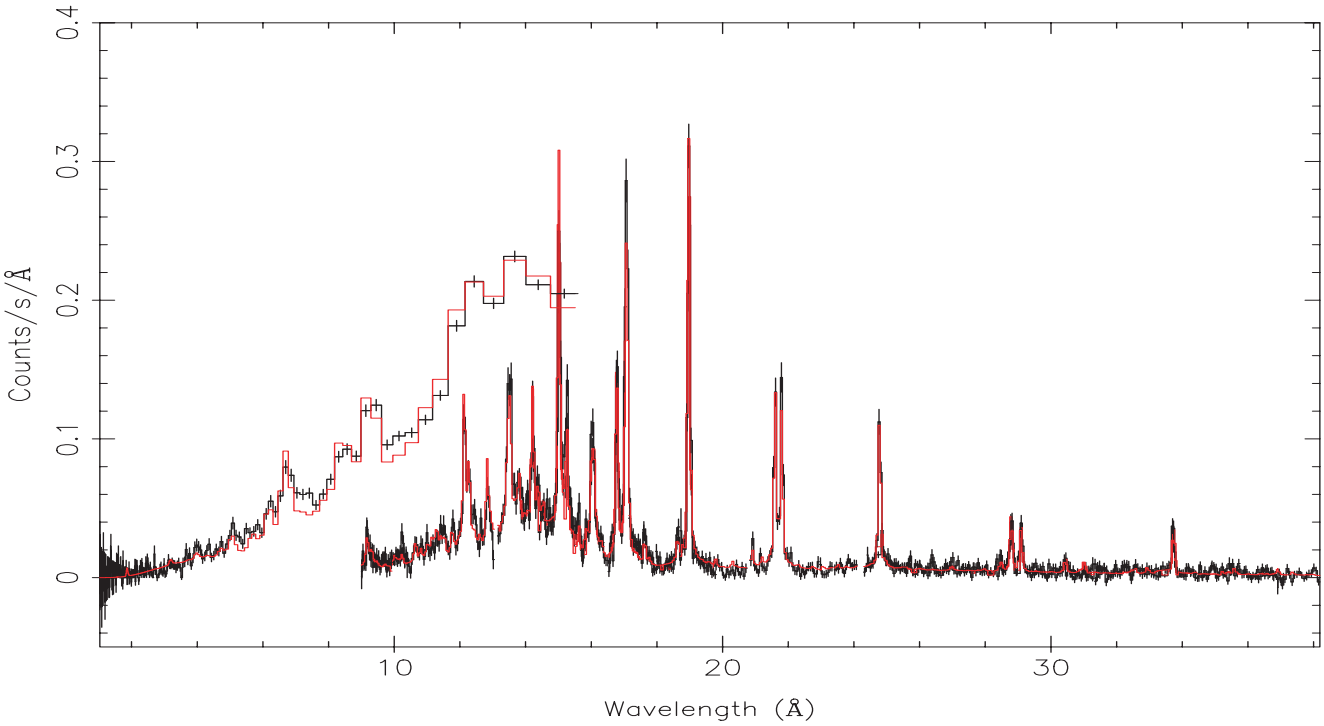

Fig. 3. RGS (rebinned by factor 5 by combining neighbouring bins and cut off below 9 Å) and EPIC-MOS (rebinned by factor 3 and cut off above 15.5 Å) spectra of τ Sco compared with best-fit 4T model (red line).

(1.86 Å) that is too weak to be detected above the background for the EPIC-MOS instrument (cf. also Table 1) (further rebinning below 2 Å did not reveal any observed Fe 6.7 keV line feature).

We have also made an attempt to fit only the EPIC spectrum below 10 Å. We fixed the first 3 components and the abundances below Mg and replaced the 4th component by two free hot components 4 & 5. Then we obtained for the latter two: $T_4 = 13$, $EM_4 = 3.3$, $T_5 = 20$, $EM_5 = 1.7$ (same units as in Table 2) and within the uncertainties the same abundances except for Ar where we now obtain an abundance of 1.5× solar, and a better fit to the Ar XVII line. It turns out that in the 5-T model the Fe 6.7 keV line becomes even weaker (~3×), i.e. 5× below the observed 2σ upper limit.

Non-thermal emission? The detection of many lines that are well fit by the three softer temperature components suggests that this part of the X-ray emission is due to a multi-temperature, *thermal* plasma. The question is whether the high-energy ($\gtrsim$10 MK) emission is thermal or non-thermal. In the latter case, the hard X-ray photons could be produced by inverse Compton scattering of stellar UV photons on relativistic shock-accelerated particles in the wind. Such a model was applied to OB supergiants but may be also of relevance to other hot stars that are subject to radiation line-driven instabilities (e.g., Chen & White 1991; Skinner et al. 2002). To investigate the possibility of a power-law model, we have fitted a model with the three lower temperature components plus a power-law component having a low-energy cutoff at e.g., $E = 1$ keV. It turns out that the norm of the power-law component tends to zero as the fit progresses. We conclude that our observations (which become noisy above about 2 keV) do not allow us to show the presence of non-thermal emission.

Abundances. In Table 3 we give the abundance ratios with respect to iron, relative to the corresponding solar values, in order of increasing First Ionization Potential (FIP). For the solar corona elements with a low FIP ($\lesssim$10 eV) are observed to be overabundant, with respect to the photospheric abundance, whereas the high-FIP elements are relatively underabundant. This dependence of the abundance on the first ionization potential is called the "FIP" effect (e.g., Feldman et al. 1992). The abundance ratios in Table 3 may suggest such a trend for τ Sco, i.e. diminishing A/Fe with increasing FIP. However, given the errors in Table 3, we cannot conclude this. But a striking result is the clear overabundance of the high-FIP element nitrogen. The ratio N/Fe is supersolar both for the shocks in the wind (~2.6×) and for the photosphere (~1.6×) (cf. Table 2). For the N/O ratio we have ~3.3× and ~2.4×, respectively.

3.3.2. Differential emission measure (DEM) modelling

To show the relative importance of the different temperature components we applied a differential emission measure (DEM) model of the stellar wind X-ray source of τ Sco using the various inversion techniques offered by SPEX (see Kaastra et al. 1996b). We define the DEM by $n_e n_H dV/d\log T$ (integrated over one logarithmic temperature bin $EM = n_e n_H V$). In Fig. 4 we show the resulting EM obtained from a simultaneous fitting of the RGS and EPIC spectra either with the regularization algorithm ($\chi^2 = 1596$) or with a polynomial of order 8 ($\chi^2 = 1718$).

Table 2. Best-fit parameters for a 4-T CIE model fit. Values are given with 1σ uncertainties. Elemental abundances are given relative to solar photospheric values (Anders & Grevesse 1989), except for Fe[a].

Parameter	RGS+MOS	phot. abund.[b]
log $N_{\rm H}$ [cm^{-2}]	20.5[c]	
T_1 [MK]	1.64 ± 0.06	
T_2 [MK]	5.7 ± 0.1	
T_3 [MK]	8.4 ± 0.9	
T_4 [MK]	20 ± 1	
EM_1 [10^{53}cm^{-3}]	3.4 ± 0.3	
EM_2 [10^{53}cm^{-3}]	6.3 ± 0.6	
EM_3 [10^{53}cm^{-3}]	6.3 ± 0.4	
EM_4 [10^{53}cm^{-3}]	3.5 ± 0.3	
$L_{\rm x}$[d] [10^{31} erg/s]	3.24[d]	
Abundances:		
C	0.48 ± 0.08	0.72
N	2.2 ± 0.3	1
O	0.70 ± 0.06	0.50
Ne	0.6 ± 0.1	1.26
Mg	1.1 ± 0.1	1.35
Si	1.1 ± 0.1	1.15
S	0.6 ± 0.1	0.76
Ar	0.6 ± 0.3	
Fe	0.9 ± 0.5	0.74
$\chi^2_{\rm red}$	1595/1020	

[a] Solar photospheric values in logarithmic units, with $\log_{10}$H = 12.00; C = 8.56; N = 8.05; O = 8.93; Ne = 8.09; Mg = 7.58; Si = 7.55; S = 7.21; Ar = 6.56; Fe = 7.50 (Grevesse & Sauval 1998, 1999).

[b] Photospheric abundances of τ Sco from Kilian (1994) relative to solar values (given in note [a]).

[c] See Diplas & Savage (1994).

[d] X-ray luminosity in the *XMM* band (0.3–10 keV) at distance d = 132 pc. Using the same units for easy comparison, the X-ray luminosity of our spectral fit is 1.86 in the *ASCA* (0.8–10 keV) band and 4.0 in the *ROSAT* (0.1–2.4 keV) band, respectively.

Table 3. Abundance ratios [A/Fe] relative to Fe in dependence of FIP.

Element	A/Fe	FIP (eV)
Mg	1.3 ± 0.9	7.64
Fe	1	7.87
Si	1.3 ± 0.8	8.15
S	0.7 ± 0.4	10.40
C	0.6 ± 0.4	11.30
O	0.8 ± 0.5	13.60
N	2.5 ± 1.7	14.50
Ar	0.7 ± 0.5	15.80
Ne	0.7 ± 0.6	21.60

The results are compatible. We assumed the same abundances as were obtained in the 4-T fit and also the same $N_{\rm H}$. As can be seen, the emission is concentrated in about the same temperature intervals as found in the 4-T fit: 1–2 MK, 4–11 MK, and 20–40 MK. The emission measures are in good agreement with the values obtained from the multi-temperature fit. The hottest component which was found earlier by Cohen et al. (1997b) from the *ASCA* spectrum (their component T_3) is confirmed in our observations. Our middle component between 4 and 11 MK contains the two lower components found by Cohen et al., while our soft component around 1–2 MK was not detectable by *ASCA*.

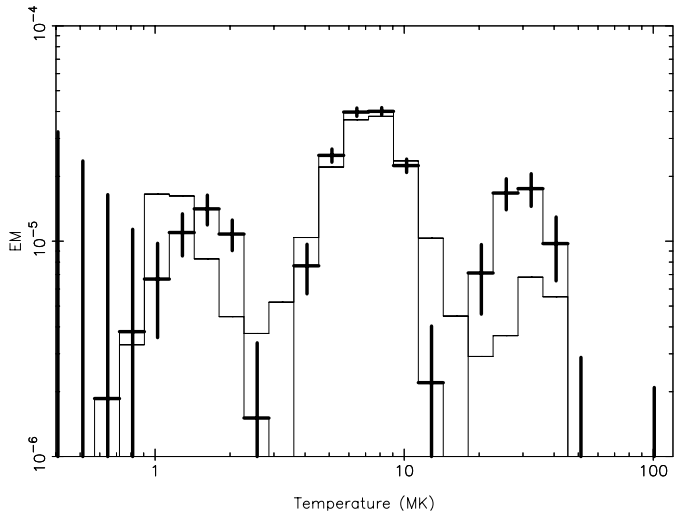

Fig. 4. Emission measure EM ($=n_e n_{\rm H} V$ per logarithmic temperature bin) (in units of 10^{58} cm^{-3}) of τ Sco derived from a fit to the RGS and EPIC-MOS spectra; EM resulting from a fit with the regularization method is shown by the thick line, and the fit with the polynomial method is shown by the thin line.

4. A model for τ Sco

It is commonly assumed that single OB and WR stars emit X-rays by shocks formed in the wind as a result of radiation line-driven instabilities (Lucy & White 1980; Lucy 1982; Owocki et al. 1988; Feldmeier et al. 1997). The soft X-rays (<10 MK) as observed from O-type stars as θ^1 Ori C (Schulz et al. 2000), ζ Ori (Waldron & Cassinelli 2001), and ζ Pup (Kahn et al. 2001; Cassinelli et al. 2001) and the soft component of τ Sco can be explained by this model. However, the hard (20–40 MK) component observed in τ Sco is not predicted by the instabilities in the radiation line-driven model, so a different mechanism is required to explain how such hard emission can arise.

Recently Howk et al. (2000) developed a model for τ Sco's wind to explain the hard ($\gtrsim$20 MK) emission. In their model it is assumed that clumps form by line-driven wind instabilities and the large density increase in the cooling region in shock zones, as was shown in the shock model for τ Sco developed by MacFarlane & Cassinelli (1989).

The line force in hot star wind simulations depends on the velocity gradient in a wind, dv/dr. However, within a clump there is a plateau in the velocity distribution and the line force becomes negligible. Thus the clumps tend to lag behind the ambient wind and if their velocity is less than the velocity of escape and if the other outward forces are small the clumps could even fall back toward the star. In Howk et al. (2000) trajectories are calculated accounting for the outward force of

drag by the ambient wind, the continuum radiation forces on the optically thick clump, and the inward force of gravity. It was found that for the wind of τ Sco and for clump masses in the range of about 10^{19} to 10^{20} g, the clumps would stall and fall back toward the star, and there would be a bow shock interface with the incident wind. The infall can explain two properties of τ Sco: the peculiar redshifted component seen in the profiles of the O VI and N V superionization spectral lines in the Copernicus spectrum (Lamers & Rogerson 1978), and the anomalously hard and strong X-ray emission from this star as observed by *ROSAT* and *ASCA*. From the depth of the observed redward shifted component of the O VI λ1038 Å absorption line, Howk et al. (2000) estimated that the clumps cover about 10% of the surface of the star. The hard X-ray spectrum can be explained by the fact that there is a larger jump in velocity across a shock. The larger velocity jump can be produced in a case where the collision is with clumps that are moving slowly relative to the wind or are falling back toward the star. With *XMM-Newton*, we have a broader range of energy coverage and a higher spectral resolution than *ROSAT* and *ASCA*, so we can re-address the Howk et al. model and obtain improved information on temperatures, the X-ray source location, and speed distributions. There are three peculiar properties of the *XMM-Newton* spectra of τ Sco, that can perhaps be explained by bow shocks and clumps in the wind:

a) The maximum temperature derived from the hard component is large and is seen to be about 40 MK from Fig. 4.

b) The f/i line ratio for one of the highest helium-like ions seen (Mg XI) indicates (see Fig. 2) that the lines form in the region from the stellar surface out to 4 stellar radii. In at least the inner part of this range the wind speeds tend to be relatively small.

c) The lines show a Doppler broadening that is narrower than the lines seen in other hot stars measured with *XMM* or *Chandra* and the lines are near rest velocity. These properties of the lines mean that the source of the X-ray lines is moving slowly relative to the star, as is true for the nearly stationary or slowly infalling clumps.

Measurable Doppler shifting to the shorter wavelengths and broadening would tend to occur if the X-rays are formed in shocks moving in the radial outward direction (Cassinelli et al. 2001). Further evidence for the low speeds of the X-ray line forming regions in τ Sco are given by Cohen et al. (2002), in which *Chandra* observations are analyzed.

A bow shock shows a range in shock temperatures, but the maximal temperature contains the most direct information about the incident flow. This is because the maximal temperature occurs at the peak of the bow shock, and its value is set by the classical Rankine-Hugoniot relation, $kT_s = (3/16)\bar{m}\Delta v^2$ (with mean mass $\bar{m} = 0.619 m_p$ for a helium abundance He/H = 0.1 and full ionization of H and He). The temperature T_s behind a strong adiabatic shock is numerically given by

$$T_s(\mathrm{MK}) = 14\,[\Delta v(1000\ \mathrm{km\ s^{-1}})]^2, \quad (1)$$

where $\Delta v = v_{\rm wind} - v_{\rm clump}$ is the shock jump velocity. The temperature in Eq. (1) should be considered as a maximum in the clump model and is given by the upper temperature cutoff of the DEM analysis (Fig. 4). The temperature (30 MK) of the peak of the hot component (cf. Fig. 4) combined with Eq. (1) gives a relative velocity Δv of about 1500 km s^{-1}.

The velocity distribution in the wind of τ Sco is taken in Howk et al. (2000) to be given by the beta velocity law

$$v = v_\infty\,(1 - R_*/r)^\beta, \quad (2)$$

where $\beta = 0.8$ (Groenewegen & Lamers 1989) and the terminal velocity is $v_\infty = 2400$ km s^{-1} (Howk et al. 2000). With this distribution the wind speed would reach about 1500 km s^{-1} at a radial distance of $r = 2.25R_*$. In the usual picture of the formation of X-rays derived from one-dimensional hydrodynamical models of unstable winds such as that in Cooper & Owocki (1994), the shock velocity jump is typically about half the local wind speed. So for those models it would be difficult to reach the required velocity jumps and the high temperatures derived from the DEM analysis anywhere in the wind of τ Sco. In the clump model, even negative source velocities are possible, and the negative velocities of the infalling Howk et al. clumps can be a few hundred km s^{-1}, thus the shock jump velocity should be the local wind speed plus the infall speed. Furthermore, the high relative velocity can be reached at radii less than about $2R_*$.

As an example consider a simple picture of many clumps of mass 10^{19} g, all located at $2R_*$. Using the assumptions and equations in Howk et al. we find that a jump velocity of 1500 km s^{-1} corresponds to an infall speed of about –90 km s^{-1}, far below our velocity resolution of 400 km s^{-1}. To produce a hard component X-ray luminosity of 6×10^{30} erg s^{-1} nearly 1000 clumps are required, and this is comparable to the number of clumps discussed in the paper by Howk et al. regarding the O VI coverage and X-ray luminosities. If we take their result that the clumps have trajectory times of about 7 hours, the total mass in the 1000 clumps is about 25% the mass outflow in the wind in that time. These numerical estimates are all in the "plausible" regime, but of course more detailed modelling is required to test the clump and any other X-ray model for τ Sco.

5. Discussion and conclusions

5.1. Line broadening and loci of hot shocks

Spectral lines of the O4 f star ζ Puppis measured by *XMM-Newton* RGS (Kahn et al. 2001) and by *Chandra* MEG and HEG (Cassinelli et al. 2001) show a significant line broadening corresponding to velocities of up to about 1500 km s^{-1}. This value is close to the terminal wind velocity of the star (2200 km s^{-1}) which implies that the lines must be formed far out in the wind of ζ Pup.

On the other hand, as compared with the *XMM-Newton* observations of Kahn et al. (2001) the linesin our measured spectrum of τ Sco (cf. Fig. 1) are much narrower, so narrow that no broadening is observed here. The observed line profile is consistent with the instrumental profile of $FWHM$ of about 0.07 Å (hence $\Delta\lambda_{\rm line} \lesssim 0.03$ Å), which implies that the lines must be formed in a region where the X-ray source speed is smaller than about 500 km s^{-1}, which is much smaller than the terminal velocity (2400 km s^{-1}). That this occurs relatively close to the

star is also indicated by the results derived from the f/i ratios (see Sect. 3.2).

The difference between τ Sco and ζ Pup can be explained by the widely different mass loss rates for these two stars (3×10^{-8} and 5×10^{-6} $M_{\odot}$ yr^{-1}, respectively). One can expect that the wind of ζ Pup is optically thick to X-rays over a much larger distance than for τ Sco so that the X-ray spectral lines of ζ Pup are formed high up in the wind, whereas the lines from τ Sco are formed much closer to the stellar surface.

In this low region of the wind of τ Sco radiation line-driven instabilities could produce shocks (in a similar way as in the more massive winds of OB giants and O main-sequence stars) with temperatures on the order of a few MK ($\Delta v \lesssim 500$ km s^{-1}) (cf. Eq. (1)). This could explain the observed soft X-ray component ($\lesssim$10 MK) (cf. Table 2 and Fig. 4), as was argued for τ Sco by Cohen et al. (1997b) and Howk et al. (2000).

The observed hard component ($\gtrsim$10 MK) is explained by dense clumps stalling and falling back and producing in the ambient wind a hot bow shock with relative velocities up to about 2000 km s^{-1}.

5.2. Large N abundance; comparison with ζ Pup

The *XMM-Newton* RGS and *Chandra* MEG spectra of ζ Pup (Kahn et al. 2001 and Cassinelli et al. 2001, respectively) and our RGS spectrum of τ Sco (Fig. 1) show that the N VI & N VII lines are prominent relative to the O VII & O VIII and C VI lines. The overabundance of nitrogen is given by a high ratio of N/O ($\gtrsim 10 \times$ solar for ζ Pup and $\sim 3 \times$ solar for τ Sco). For ζ Pup this strong overabundance could be explained by the large mass loss rate to strip down to the CNO burning region. But for τ Sco it is not very probable that the material has undergone CNO processing because the mass loss rate of this star is two orders of magnitude smaller. Here we assume that the relative N/O overabundance is primordial rather than due to the processing effect.

5.3. Presence of hot gas in other early-type stars

The *Chandra* high-resolution spectrum of ζ Ori (O 9.5 Ia) was found by Waldron & Cassinelli (2001) to have a high ionization state of Si XIII very near to the star, to have symmetric and unshifted line profile shapes, and to have a line formation region very close to the star. They suggested that the star must have anomalously hot gas close to the star and perhaps confined in magnetic loops. Similar properties were found for highly ionized atoms in ζ Pup (O4f) by Cassinelli et al. (2001).

Recently Skinner et al. (2002) have measured with the EPIC-PN on *XMM-Newton* and the *VLA* the presumably single Wolf-Rayet star WR 110. The emission measure distribution shows a dominant contribution from relatively cool plasma of temperature 6 MK analogous to the 5–8 MK component for τ Sco. In addition, a hard X-ray component was detected on WR 110. *VLA* observations seem to rule out the interpretation of non-thermal emission for this component (non-detection of relativistic particles) and it is believed that the hard X-rays are more likely to originate from a thermal ($\gtrsim$40 MK) plasma comparable to the hot component of τ Sco. This hard emission is not anticipated on the basis of current radiation line-driven wind shock models for single hot stars. Instead of a model involving clumps, Skinner et al. (2002) have proposed that the hard emission arises from the wind shocking onto an, as yet undetected, close companion.

In both τ Sco and in WR 110 the observations did not allow for the detection of Fe K emission. However, we remark that in some well-studied WR+OB colliding-wind binaries such as WR 140 (Koyama et al. 1994), γ^2 Vel (Skinner et al. 2001), and WR 25 (Raassen et al. 2002) Fe K emission has been clearly detected. So in these cases the very hot plasma seems to be the result of the interaction between the colliding winds in the WR+OB binaries.

However, there are several important differences between τ Sco and the WR stars. Most importantly, as mentioned before, τ Sco shows clear evidence for a downward component of the O VI and N V resonance line profiles in the UV. The wind of τ Sco is optically thin so that we can detect X-rays even from deep in the wind, whereas for the WR stars the winds are extremely thick to X-rays and we are able to study only emission from the outer parts of their winds. τ Sco is a very well studied star with sharp photospheric lines, so a companion would likely have been detected. Given these considerations, it appears that *XMM-Newton* is providing support for the presence of clumps in τ Sco.

In summary, the possibility of the stalling or infalling of the clumps allows for a large shock jump velocity ($\gtrsim$1500 km s^{-1}). The resultant X-ray lines can be formed near the star as is required by the f/i analysis of the He-like ions. The low velocity of the clumps relative to the star, can explain why the X-ray lines do not show significant Doppler shifting or broadening.

It is interesting to ask if the clump phenomenon is of importance for other early-type stars. One of the odd results derived from observations of other hot stars by *XMM-Newton* and *Chandra* is that, with the exception of ζ Pup, the X-ray emission lines are not significantly displaced from the line center, nor are the line profiles skewed as would be expected if the X-ray emission arose in shocks participating in the bulk motion of the wind. Perhaps the winds have clumps analogous to what we are finding in τ Sco, although the drag forces are much larger in stars with larger mass loss rates, so there should be significant differences from τ Sco.

Acknowledgements. The National Institute for Space Research (SRON) is supported financially by NWO. The PSI group acknowledges support from the Swiss National Science Foundation (grant 2000-058827.99). JPC and NAM acknowledge support from NASA grants NAG5 5-9226 and GO2-3028, respectively. We are grateful to the calibration teams of the instruments on board *XMM-Newton*. Finally, we would like to thank the referee Dr. A. Feldmeier for many useful remarks.

References

Anders, E., & Grevesse, N. 1989, Geochim. Cosmochim. Acta, 53, 197

Blumenthal, G. R., Drake, G. W. F., & Tucker, W. H. 1972, ApJ, 172, 205

Cassinelli, J. P., Cohen, D. H., MacFarlane, J. J., Sanders, W. T., & Welsh, B. Y. 1994, ApJ, 421, 705

Cassinelli, J. P., Miller, N. A., Waldron, W. L., MacFarlane, J. J., & Cohen, D. H. 2001, ApJ, 554, L55
Cassinelli, J. P., & Olson, G. L. 1979, ApJ, 229, 304
Chen, W., & White, R. L., ApJ, 366, 512
Cohen, D. H., Cassinelli, J. P., & MacFarlane, J. J. 1997a, ApJ, 487, 867
Cohen, D. H., Cassinelli, J. P., & Waldron, W. L. 1997b, ApJ, 488, 397
Cohen, D. H., de Messières, G. E., MacFarlane, J. P., et al. 2002, ApJ, submitted
Cooper, R. G., & Owocki, S. P. 1994, Ap&SS, 221, 427
Diplas, A., & Savage, B. P. 1994, ApJS, 93, 211
Feldman, U., Mandelbaum, P., Seely, J. F., Doschek, G. A., & Gursky, H. 1992, ApJS, 81, 387
Feldmeier, A., Puls, J., & Pauldrach, A. W. A. 1997, A&A, 322, 878
Gabriel, A. H., & Jordan, C. 1969, MNRAS, 145, 241
Grevesse, N., & Sauval, A. J. 1998, Space Sci. Rev., 85, 161
Grevesse, N., & Sauval, A. J. 1999, A&A, 347, 348
Groenewegen, M. A. T., & Lamers, H. J. G. L. M. 1989, A&A, 79, 359
den Herder, J. W., Brinkman, A. C., Kahn, S. M., et al. 2001, A&A, 365, L7
Howk, J. C., Cassinelli, J. P., Bjorkman, J. E., & Lamers, H. J. G. L. M. 2000, ApJ, 534, 348
Jansen, F., Lumb, D., Altieri, B., et al. 2001, A&A, 365, L1
Kaastra, J. S., Mewe, R., & Nieuwenhuijzen, H. 1996a, in UV and X-ray Spectroscopy of Astrophysical and Laboratory Plasmas, ed. K. Yamashita, & T. Watanabe (Universal Academy Press, Inc., Tokyo), 411 (SPEX)
Kaastra, J. S., Mewe, R., Liedahl, D. A., et al. 1996b, A&A, 314, 547
Kahn, S. M., Leutenegger, M. A., Cottam, J., et al. 2001, A&A, 365, L312
Kelly, R. L. 1987, Atomic and Ionic Spectrum lines below 2000 Angstroms: Hydrogen through Krypton, J. Phys. Chem. Ref. Data 16, suppl. 1
Kilian, J. 1994, A&A, 282, 867
Koyama, K., Maeda, Y., Tsuru, T., Nagase, F., & Skinner, S. 1994, PASJ, 46, L93
Kurucz, R. L. 1993, in Peculiar versus Normal Phenomena in A-Type and Related Stars, ed. M. M. Dworetsky, F. Castelli, & R. Faraggiana (San Francisco: ASP), ASP Conf. Ser., 44, 87
Lamers, H. J. G. L. M., & Rogerson, J. B. 1978, A&A, 66, 417
Lucy, L. B., & White, R. L. 1980, ApJ, 241, 300
Lucy, L. B. 1982, ApJ, 255, 286
MacFarlane, J. J., & Cassinelli, J. P. 1989, ApJ, 347, 1090
Mewe, R., Gronenschild, E. H. B. M., & van den Oord, G. H. J. 1985, A&AS, 62, 197 (MEKAL)
Mewe, R., Kaastra, J. S., & Liedahl, D. A. 1995, Legacy, 6, 16 (MEKAL)
Owocki, S. P., Castor, J. I., & Rybicki, G. B. 1988, ApJ, 335, 914
Perryman, M. A. C., & the *Hipparcos* Science Team 1997, The *Hipparcos* and Tycho Catalogues, ESA report SP-1200 (Noordwijk: ESA)
Porquet, D., Mewe, R., Dubau, J., Raassen, A. J. J., & Kaastra, J. S. 2001, A&A, 376, 1113
Raassen, A. J. J., van der Hucht, K. A., Mewe, R., et al. 2002, in preparation
Schulz, N. S., Canizares, C. R., Huenemoerder, D., & Lee, J. C. 2000, ApJ, 545, L135
Skinner, S. L., Güdel, M., Schmutz, W., & Stevens, I. R. 2001, ApJ, 558, L113
Skinner, S. L., Zhekov, S. A., Güdel, M., & Schmutz, W. 2002, ApJ, 572, 477
Strüder, L., Briel, U. G., Dennerl, K., et al. 2001, A&A, 365, L18
Turner, M. J. L., Abbey, A., Arnaud, M., et al. 2001, A&A, 365, L27
Walborn, N. R., & Fitzpatrick, E. L. 1990, PASP, 102, 379
Waldron, W. L., & Cassinelli, J. P. 2001, ApJ, 548, L45
Zaal, P. A., de Koter, A., Waters, L. B. F. M., et al. 1999, A&A, 349, 573